A New Algorithm to Represent Texture Images

Silvia María Ojeda
Facultad de Matemática, Astronomía y Física
Universidad Nacional de Córdoba
Córdoba, Argentina

Grisel Maribel Britos
Facultad de Matemática, Astronomía y Física
Universidad Nacional de Córdoba
Córdoba, Argentina

***Abstract*—In recent times the spatial autoregressive models have been extensively used to represent images. In this paper we propose an algorithm to represent and reproduce texture images based on the estimation of spatial autoregressive processes. The image intensity is locally modeled by a first spatial autoregressive model with support in a strongly causal prediction region on the plane. A basic criteria to quantify similarity between two images is used to locally select this region among four different possibilities, corresponding to the four strongly causal regions on the plane. Two global image similarity measures are used to evaluate the performance of our proposal.**

Keywords—Autoregressive Models; Texture Images; Similarity Measures.

I. INTRODUCTION

The goal of this work is to introduce a new algorithm to represent and reproduce texture images that uses and improves other recent proposals concerning this topic.

Most of the images of interest, for example, the images of cultivated fields and concentration of population are naturally rich in texture, level of gray, etc. The same thing happens to the images of geographical regions that allow the making of maps and, in general, almost all the images of the earth. During the past decades, image representation and image texture recovery have been two important and challenging topics. In this sense the spatial autoregressive model (AR- 2D model) has been extensively used to represent images ([3], [14]) due to its two main properties. First, simulation experiments have shown that this model is adequate to represent a diversity of real scenarios ([4]). Second, the AR-2D model does not require a large number of parameters to represent different real scenarios (parsimony) ([4]). In particular, the first-order AR-2D model is able to represent a wide range of texture images, as is shown in Figure 1; the image (a) have been generated by a first-order AR-2D model with three parameters, while images (b), (c), (d) and (e) have been generated by a model of the same type with two parameters. Theoretical properties of the first-order AR-2D model were studied by Basu and Reinsel ([2]). They derived the correlation structure of the model and the maximum likelihood estimators of the parameters. Also, the spatial autoregressive models have benefited other topics in image processing like image segmentation. An approach to perform image segmentation based on the estimation of AR-2D processes has been recently suggested by Ojeda et al. ([15]). First an image is modeled using a spatial autoregressive model for the image intensity. Then the residual autoregressive image is computed. This resulting image possesses interesting texture features. The borders and edges are highlighted, suggesting that the algorithm can be used for border detection. Later, a new scheme was proposed to enhance the segmentation yielded by the previous algorithm (Vallejos et al., 2012, [18]). It is based on the identifying of the best prediction window, and generalizes the previous algorithm to different prediction windows associated with unilateral processes on the plane. An analysis of the association between the original and fitted images shows how the algorithm works in practice. In all experiments carried out in [18], the first step of the segmentation algorithm was implemented using the same strongly causal prediction window. Consequently the support of the the local autoregressive models used to represent the images was always the same. Our proposal is a methodology that allows to identify locally the strongly causal prediction window (and consequently the support of the first-order AR-2D processes) associated with the better local representation of the image. To analyze the performance of our method, we quantified the similarity between the original and fitted images by two image measures. The study shows that the new method is capable to enhance the capacity of the AR-2D models to reproduce and represent images.

The rest of the paper is organized as follows: Section II presents a brief description of most used schemes of neighborhoods in $\mathbb{Z}^2$. Section III provides an overview of the spatial ARMA models. Section IV presents the recent algorithm developed by Ojeda et al. ([15]) and the improvement due to Vallejos et al. ([18]) in the context of image segmentation. In Section V we explain our proposal to reproduce and represent texture images based on the estimation of spatial autoregressive processes. Section VI shows the results of our study and provides an analysis of the performance of our methodology using two similarity image measures. Conclusions and future scopes will appear in sections VII and VIII respectively.

II. NEIGHBOROODS IN $\mathbb{Z}^2$

In time series, there is a natural neighbor structure induced by the existing total order of Z (the set of all past values of $t \in \mathbb{Z}$; is the set of all integers that are less than t). However, for points on the plane, for instance $(m,n) \in \mathbb{Z}^2$, there are several different notions of neighborhood.

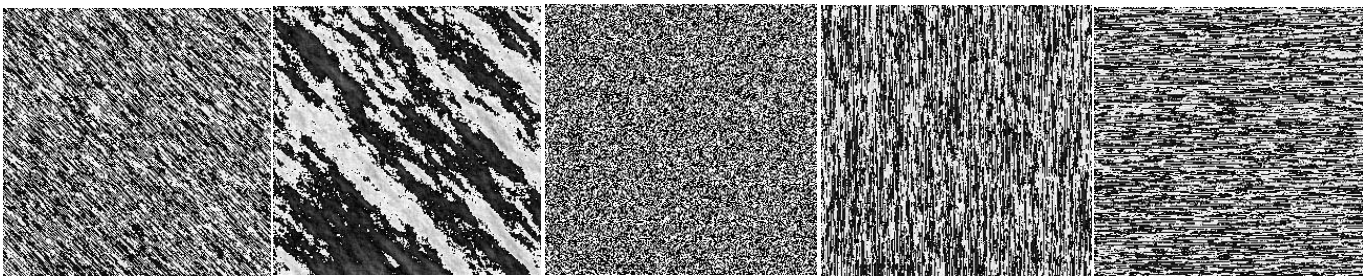

(a) (b) (c) (d) (e)

Fig. 1 Texture images generated by AR-2D process: (a) $\phi_1 = 0.0100$, $\phi_2 = 0.0100$, $\phi_3 = 0.8000$; (b) $\phi_1 = 0.5000$, $\phi_2 = 0.4999$; (c) $\phi_1 = 0.0100$, $\phi_2 = 0.0200$; (d) $\phi_1 = 0.0100$, $\phi_2 = 0.9000$; (e) $\phi_1 = 0.9000$, $\phi_2 = -0.0200$

In general, definitions of neighborhood of a point (m,n) on the plane are motivated by the physical acquisition system of the data like in the case of images that have been captured by satellites. A description of the most commonly used neighbor structures in statistical image processing can be found in [13]. In this paper we define the structure of neighborhood based on strongly causal regions.

For all $(m,n) \in \mathbb{Z}^2$ we distinguish the following strongly causal regions:

$$S_1(m,n) = \{(k,l) \in \mathbb{Z}^2 : k \le m, l \le n\} - \{(m,n)\}$$
$$S_2(m,n) = \{(k,l) \in \mathbb{Z}^2 : k \ge m, l \le n\} - \{(m,n)\}$$
$$S_3(m,n) = \{(k,l) \in \mathbb{Z}^2 : k \ge m, l \ge n\} - \{(m,n)\}$$
$$S_4(m,n) = \{(k,l) \in \mathbb{Z}^2 : k \le m, l \ge n\} - \{(m,n)\}$$

Considering the region $S_1(m,n)$, a strongly causal prediction window containing two elements is

$$W_1 = \{(k,l) \in S_1(m,n) : m-1 \le k \le m, n-1 \le l \le n\} - \{(m-1, n-1)\}$$

W_1 is shown in Figure 2 (a). Similarly, the strongly causal prediction windows W_2, W_3, and W_4, with two elements each, can be defined considering $S_2(m,n)$, $S_3(m,n)$ and $S_4(m,n)$ respectively (Figure 2, (b)-(d)).

III. SPATIAL ARMA MODELS

Spatial ARMA processes have also been studied in the context of random fields indexed over $\mathbb{Z}^d$, $d \ge 2$, where $\mathbb{Z}^d$ is endowed with the usual partial order; that is, for $s = (s_1, s_2, \dots, s_d)$, $u = (u_1, u_2, \dots, u_d)$ in $\mathbb{Z}^d$, $s \le u$ iff for $i = 1,2,\dots,d$, $s_i \le u_i$. Let $S[a,b] = \{x \in \mathbb{Z}^d : a \le x \le b\}$

and $S(a,b] = S[a,b]/\{a\}$, where $a, b \in \mathbb{Z}^d$; $a \le b$ and $a \ne b$. A random field $(X_s)_{s\in\mathbb{Z}^d}$ is said to be a spatial ARMA (p,q) with parameters $p, q \in \mathbb{Z}^d$ if it is weakly stationary and satisfies the equation

$$X_s = \sum_{j\in S(0,p]} \phi_j X_{s-j} + \sum_{k\in S(0,q]} \vartheta_k \varepsilon_{s-k} + \varepsilon_s \qquad (1)$$

where $(\phi_j)_{j\in S(o,p]}$ and $(\vartheta_k)_{k\in S(o,q]}$ denotes, respectively the autoregressive and moving average parameters with $\phi_0 = \vartheta_0 = 1$; and $(\varepsilon_s)_{s\in\mathbb{Z}^d}$ denotes a sequence of independent and identically distributed centered random variables with variance σ^2. Notice that if $p = 0$, the sum over $S(0,p]$ is supposed to be zero and the process is called spatial moving average MA(q) random field,

$$X_s = \sum_{k\in S(0,q]} \vartheta_k \varepsilon_{s-k} + \varepsilon_s \qquad (2)$$

Similarly if $q = 0$ the process is called spatial autoregressive AR(p) random field, and it is defined as:

$$X_s = \sum_{j\in S(0,p]} \phi_j X_{s-j} + \varepsilon_s \qquad (3)$$

The ARMA random field is called causal if it has the following unilateral representation

$$X_s = \sum_{j\in S[0,\infty]} \psi_j \varepsilon_{s-j} \qquad (4)$$

with $\sum_j |\psi_j| < \infty$. Similarly to the time series case, there are conditions for the (AR or MA) polynomials to have stationarity and invertibility respectively. Let $\Phi(z) = 1 - \sum_{j\in S(0,p]} \phi_j z^j$ and $\Phi(z) = 1 - \sum_{j\in S(0,q]} \vartheta_j z^j$, where $z = (z_1, z_2, \dots, z_d)$ and $z^j = z_1^{j_1} z_2^{j_2} \dots z_d^{j_d}$. A sufficient condition for the random field to be causal is that the AR polynomial $\Phi(z)$ has no zeros in the closure of the open disc D^d in $\mathbb{C}^d$.

Applications of spatial ARMA processes and the study of spatial unilateral first order ARMA model have been developed in [10], [7], [2]. Other extensions of the theory developed for time series to spatial ARMA models can be found in [11], [6], [1], [17], [9], [5], [8]. As an example, consider a particular case of model (3) when $d = 2$ and $p = (1,1)$. This model is called a first-order autoregressive process. In this case, $S\big((0,0),(1,1)\big] = \{(0,1),(1,1),(1,0)\}$ and the model is of the form:

$$X_{(i,j)} = \phi_{(1,0)} X_{(i-1,j)} + \phi_{(1,1)} X_{(i-1,j-1)} + \phi_{(0,1)} X_{(i,j-1)} + \varepsilon_{(i,j)}$$

Note that $\phi_{(1,1)} = 0$, implies that for all $(i,j) \in S_1(i,j)$, $W_1(i,j)$ is the strongly causal prediction window of the intensity $X_{(i,j)}$.

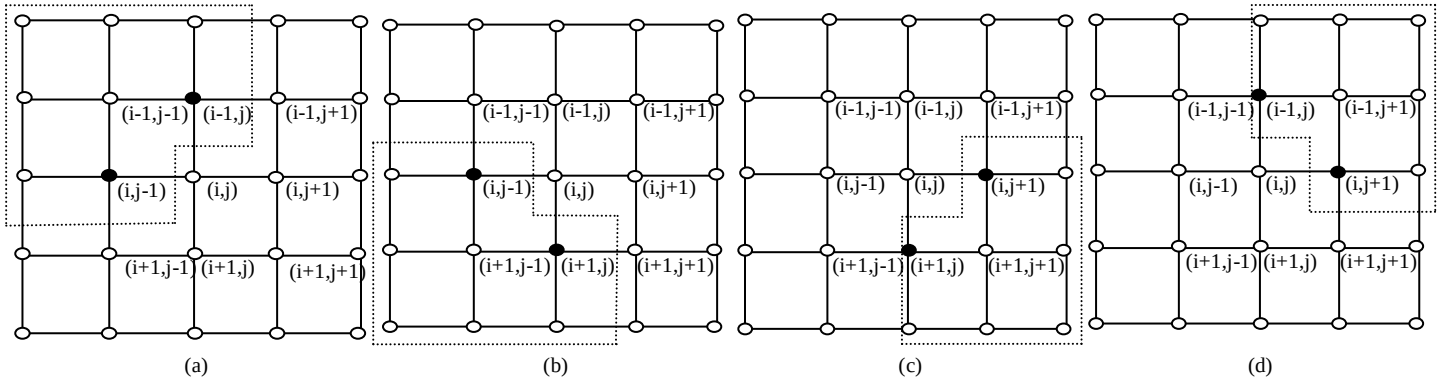

Fig. 2 Prediction windows for the first order spatial AR model with two parameters: (a) W_1, (b) W_2, (c) W_3 and (d) W_4.

IV. Approximation of Images By Using 2D Unilateral AR Processes

In this section, we describe an algorithm to approximate an image by first-order AR-2D processes whit two parameters using blocks. This algorithm was originally defined by [14] and later adapted by [15]. Following, we briefly describe this methodology.

Suppose that a real image is available. This fitted image is constructed by dividing the original image into squared sub-images (e.g., 5×5) and then fitting a first-order AR 2D model to each sub-image (i.e., block). Then, a sub-image is generated from each local fitted model and the final fitted image is yielded by putting together all generated sub-images. Let $Z = Z_{(m,n)}$, $1 \le m \le M$, $1 \le n \le N$ be the original image, and let $X = X_{(m,n)}$, $1 \le m \le M$, $1 \le n \le N$ where, for all $1 \le m \le M$, $1 \le n \le N$, $X_{(m,n)} = Z_{(m,n)} - \bar{Z}$; and $\bar{Z}$ is the mean of Z. Let $4 \le k \le min(M,N)$ (e.g. $k = 5$). For simplicity we shall consider from now on that the images to be processed (Z and X) are arranged in such a way that the number of columns and the number of rows are multiples of k; that is,

$Z = (Z_{(m,n)})$; $1 \le m \le M'$; $1 \le n \le N'$;
$X = (X_{(m,n)})$; $1 \le m \le M'$; $1 \le n \le N'$;

Where $M' = [\frac{M}{k}]k$ and $N' = [\frac{N}{k}]k$. Considering the values $M'' = [\frac{M'-1}{k-1}]$ and $N'' = [\frac{N'-1}{k-1}]$. For all $i_b = 1, \dots, M''$ and $j_b = 1, \dots, N''$, define the $k \times k$ block (i_b, j_b) of the image X by

$$B_X(i_b, j_b) = (X_{(r,s)}),$$

Where r and s are sub-index that satisfy:

$$(k-1)(i_b - 1) + 1 \le r \le (k-1)i_b + 1,$$
$$(k-1)(j_b - 1) + 1 \le s \le (k-1)j_b + 1.$$

The $M' \times N'$ approximated image $\hat{X}$ of X is provided by the following algorithm.

Algorithm 1:

1) For each block $B_X(i_b, j_b)$ compute estimators of least squared $\hat{\phi}_1^1$, $\hat{\phi}_2^1$ of ϕ_1 and ϕ_2 corresponding to the block $B_X(i_b, j_b)$ in the strongly causal prediction region S_1, using the prediction windows W_1.

2) Let $\hat{X}^1(i_b, j_b)$ be defined in the block $B_X(i_b, j_b)$ by
$\hat{X}^1(i_b, j_b)_{(r+1,s+1)} = \hat{\phi}_1^1 B_X(i_b, j_b)_{(r+1,s)} + \hat{\phi}_2^1 B_X(i_b, j_b)_{(r,s+1)}$
when $r = 1, \dots, (k-1)$ and $s = 1, \dots, (k-1)$.

3) Let $\hat{X}^1$ be defined in the block $B_X(i_b, j_b)$ by
$\hat{X}^1_{((i_b-1)(k-1)+r,(j_b-1)(k-1)+s)} = \hat{X}^1(i_b, j_b)_{(r,s)}$
with $r = 1, \dots, k$ and $s = 1, \dots, k$.

4) Define the approximated image $\hat{Z}^1$ of the original image Z as:
$\hat{Z}^1_{(m,n)} = \hat{X}^1_{(m,n)} + \bar{Z}$
with $1 \le m \le M'$ and $1 \le n \le N'$.

In order to propose a more efficient algorithm, Vallejos et al. ([18]) suggested new variants of this algorithm specially to address the problem of determining the most convenient (in terms of the quality of the segmentation) prediction window of unilateral AR-2D processes. In effect, they generalize the Algorithm 1 to different prediction windows associated with unilateral processes on the plane. Three variants of the Algorithm 1 (called **Algorithm 2**, **Algorithm 3** and **Algorithm 4**) were implemented in the strongly causal prediction regions S_2, S_3 and S_4, using the prediction windows W_2, W_3 and W_4, respectively. In each block $B_X(i_b, j_b)$, and for $t = 1,2,3,4$, we denote the output corresponding to step 2-Algorithm t, as $\hat{X}^t(i_b, j_b)$. Similarity, $\hat{X}^t$ denote the output corresponding to step 3 - Algorithm t. The computation of the distance between each filtered image and the original was be done by using Q and CQ image quality measures ([18], [19], [16]). We described briefly this measures:

Let two weakly stationary processes, $(X_s)_{s \in D}$ and $(Y_s)_{s \in D}$, $D \subset \mathbb{Z}^d$, the index Q ([19]) is

$$Q = \frac{4S_{XY}\overline{X}\overline{Y}}{(S_X^2 + S_Y^2)[\bar{X}^2 + \bar{Y}^2]} = \frac{S_{XY}}{S_X S_Y} \frac{2\overline{X}\overline{Y}}{[\bar{X}^2 + \bar{Y}^2]} \frac{2S_X S_Y}{(S_X^2 + S_Y^2)} = CMV$$

where $\bar{X}$ is the mean of $(X_s)_{s \in D}$, S_X is the standard deviation of $(X_s)_{s \in D}$, and S_{XY} is the covariance between $(X_s)_{s \in D}$ and $(Y_s)_{s \in D}$ (and similarly for Y and S_Y). The quantity $C = \frac{S_{XY}}{S_X S_Y}$ models the linear correlation between $(X_s)_{s \in D}$ and $(Y_s)_{s \in D}$, $M = \frac{2\overline{X}\overline{Y}}{[\bar{X}^2 + \bar{Y}^2]}$ measures the similarity between the sample means (luminance) of $(X_s)_{s \in D}$ and $(Y_s)_{s \in D}$, and $V = \frac{2S_X S_Y}{(S_X^2 + S_Y^2)}$ measures the similarity related to the contrast

between the images. Coefficient Q is defined as a function of the correlation coefficient; hence, it is able to capture only the linear association between $(X_s)_{s\in D}$ and $(Y_s)_{s\in D}$. The CQ index was suggested by [16] and it is defined as:

$$CQ(h) = \hat{\rho}(h)MV$$

where $\hat{\rho}(h)$ is the sample codispersion coefficient in the direction h. This index, can quantify the similarity between images that are generated using a local approximation of AR-2D processes with different window sizes. Moreover, CQ captures different levels of spatial similarity between two images by considering different directions in two-dimensional space. Note that values of Q and CQ close to 0 point out a low similarity level between two images; instead, values of $|Q|$ or $|CQ|$ close to 1, indicate a high similarity level (direct or inverse, respectively).

V. A New Algorithm To Represent Texture Images

In order to represent and reproduce texture images, we suggest a methodology that we have called Algorithm 5. As Algorithms 1-4, our proposal is also based on the idea that is advantageous approximate an image by first-order AR-2D processes using blocks, just that we introduce the possibility to select in each block the causal prediction window of the model. The goal is to get $\hat{Z}^*$, a new and better representation of the original image Z, that improves the results achieved by the algorithms 1-4. Essentially in each block, our approach selects one among the algorithms 1, 2, 3 or 4, and uses it to approximate the image in the block. Previously to defined $\hat{Z}^*$, a $M' \times N'$ approximated image $\hat{X}^*$ of X is provided by the algorithm. This selection is based on the mean square error (MSE). This basic similarity measure for images is computed from the difference of intensity, of pixel to pixel, between two images. More formally, if $(X_s)_{s\in D}$ and $(Y_s)_{s\in D}$, with $D \subset \mathbb{Z}^2$, are two weakly stationary processes,

$$MSE(X,Y) = \frac{1}{MN}\sum_{i=1}^{M}\sum_{j=1}^{N}(X_{(i,j)} - Y_{(i,j)})^2$$

More details about the MSE can be consult in [19]. In the following we describe the new algorithm.

Algorithm 5:

1) In each block $B_X(i_b, j_b)$, and for $t = 1,2,3,4$, compute the least squares estimators $\hat{\phi}_1^t$; $\hat{\phi}_2^t$ of the ϕ_1 and ϕ_2 corresponding to the block $B_X(i_b, j_b)$, in the strongly causal prediction region S_t, using the prediction windows W_t (Apply step 1-Algorithm t, with $t = 1,2,3,4$).

2) In each block $B_X(i_b, j_b)$, and for $t = 1,2,3,4$, compute $\hat{X}^t(i_b, j_b)$ (Apply step 2-Algorithm t, with $t = 1,2,3,4$).

3) In each block $B_X(i_b, j_b)$, and for $t = 1,2,3,4$, compute $MSE(\hat{X}^t(i_b, j_b), B_X(i_b, j_b))$. Choose the approximated image generated by the lowest mean square error. Denote it as $X^*(i_b, j_b)$.

4) Let $\hat{X}^*$ be defined in the block $B_X(i_b, j_b)$ by

$$\hat{X}^*_{((i_b-1)(k-1)+r,(j_b-1)(k-1)+s)} = X^*(i_b, j_b)_{(r,s)}$$

with $r = 1, \dots, k$ and $s = 1, \dots, k$.

5) The approximated image $\hat{Z}^*$ of the original image Z is: $\hat{Z}^*_{(m,n)} = \hat{X}^*_{(m,n)} + \bar{Z}$ with $m = 1, \dots, M' = [\frac{M}{k}]k$ and $n = 1, \dots, N' = [\frac{N}{k}]k$.

Note how Algorithm 5 (step 3), allows to locally identify (based on the MSE) the strongly causal prediction window associated with the more adequate local representation of the original image.

VI. Experiments And Results

In this section we developed some examples in different scenarios to explore the performance of Algorithm 5. Six real images were used, Elaine, Lenna, Peppers, Threads, Rind and Aerial (Figure 3 (a)- (f)), all taken from the USC-SIPI image database [12]. We applied the Algorithms 1 to 5, for each original image, considering a block of size 5×5, and we obtained five representations of the original image. Figure 4 shows the image representations obtained by the five methods, from the original image Elaine.

To gain insight on the quality of each image representation, the images produced by the five algorithms were compared with the original image using the similarity index Q ([19]) and CQ ([16]), described in section IV. The results are shown in TABLE I. In all cases the highest values of the image quality measures were obtained for the image representation produced by the Algorithm 5. In practice, this means that the residual image (difference between the original and the approximated) is more compatible with a null image, when the Algorithm 5 is used.

Visually, in the residual images produced from the Algorithm 5, it is more difficult to detect the patterns of the respective original images, in comparison with the residual images generated from the others methods. As an example, Figure 5 shows the residual images obtained by applying the five algorithms to the original image Elaine, and Figure 6 shows the histograms of these images. Note that the residual image produced from Algorithm 5 (Figure 5 (e)) does not highlight the original borders and boundaries because the original image and the image representation are too similar. The histogram of the image (Figure 6 (e)) confirms this fact.

The results presented in this section are not restrictive to the images treated in this paper. There is a large set of images for which the experiments developed in this article can be replicated.

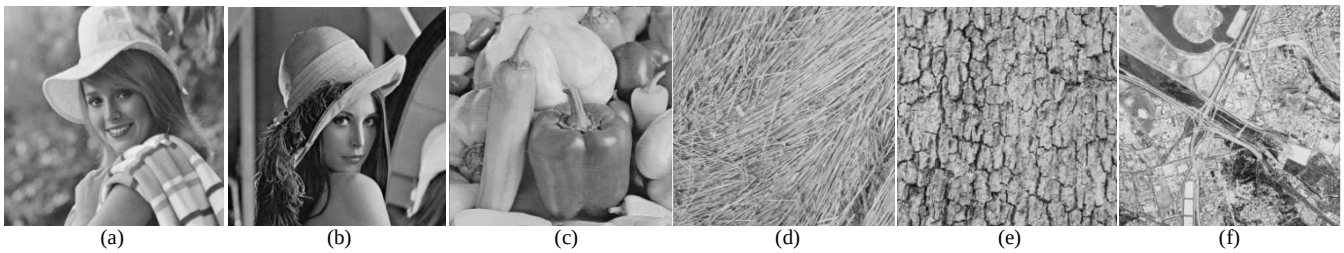

(a) (b) (c) (d) (e) (f)

Fig. 3 Images of USC-SIPI image database. (a) Elaine, (b) Lenna, (c) Peppers, (d) Threads, (e) Rind and (f) Aerial.

TABLE I. PERFORMANCE OF THE ALGORITHMS 1, 2, 3, 4, AND 5 BY Q AND CQ INDEX.

Met.	(a) Elaine		(b) Lenna		(c) Peppers		(d) Threads		(e) Rind		(f) Aerial	
	Q	CQ	Q	CQ	Q	CQ	Q	CQ	Q	CQ	Q	CQ
1	0.9769	0.5115	0.9345	0.6372	0.9895	0.8071	0.8456	0.7321	0.9155	0.6885	0.9186	0.6247
2	0.9784	0.5298	0.9529	0.6874	0.9880	0.8220	0.8804	0.7905	0.9196	0.7425	0.9154	0.6737
3	0.9780	0.5126	0.9628	0.6556	0.9877	0.8066	0.8419	0.7284	0.9193	0.6908	0.9110	0.6214
4	0.9778	0.5305	0.9472	0.6827	0.9898	0.8223	0.8782	0.7879	0.9219	0.7451	0.9059	0.6670
5	0.9878	0.7520	0.9735	0.8119	0.9947	0.8871	0.9343	0.8844	0.9579	0.8379	0.9589	0.8169

(a) (b) (c) (d) (e)

Fig. 4 (a)-(e), Image representations generated by Algorithms 1-5 respectively. Original image: Elaine.

(a) (b) (c) (d) (e)

Fig. 5 (a)-(e), Residual images (difference between the original and image representations) generated from Algorithms 1-5 respectively. Original image: Elaine.

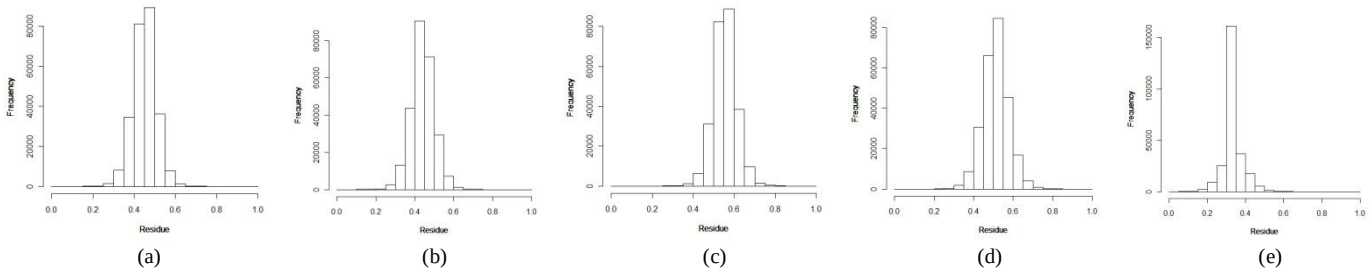

(a) (b) (c) (d) (e)

Fig. 6 a)-(e) Image residual histograms produced from Algorithms 1-5 respectively. Original image: Elaine.

VII. Conclusion

This paper proposes a new algorithm to represent and reproduce texture images based on the estimation of spatial autoregressive processes. Our proposal, as other methods, suggests approximating an image by first-order AR-2D processes using blocks, just incorporating the option to select in each block the causal prediction window of the model. This selection is based on the mean square error, a quantitative performance metric in the field of signal processing ([20]). The method, called Algorithm 5, can generate a wide range of textures using four different local approximations of AR-2D processes, corresponding to the four strongly causal regions on the plane. Using two image quality index that are extensively used in image similarity analysis, we carried out experiments that support our algorithm ([19], [20], [16]). Specifically, a set of images belonging to the image database ([12]) were processed and provided satisfactory results in order to reproduce and represent image textures. In addition the paper performs a review about the main characteristics and applications of the spatial autoregressive and moving average models. In the light of the examples presented in this article, we suggest in practice to use the Algorithm 5 as a replacement of other similar methods based on only one strongly causal region on the plane, to produce a more adequate representation of the texture images.

VIII. Future Research

The performance of the algorithm under different kinds of contamination in images is an interesting open problem to be addressed in the future. The effect of considering noncausal and semi-causal prediction windows in the spatial AR model, with different window sizes, is also an open issue to be addressed in future research.

Acknowledgment

S. Ojeda and G. Britos thank SeCyT-UNC and CIEM-FAMAF for financial assistance.

References

[1] S. Baran, G. Pap, and M. C. A. Zuijlen, “Asymptotic inference for a nearly unstable sequence of stationary spatial AR models”, Statistics & Probability Letters, Vol. 69(1), pp. 53-61, 2004.

[2] S. Basu and G. Reinsel, “Properties of the spatial unilateral first-order ARMA model”, Advances in Applied Probbability, Vol. 25(3), pp. 631-648, 1993.

[3] J. Bennet and A. Khotanzad, “Maximum likelihood estimation methods for multispectral random field image models” IEEE Transaction Pattern Analysis and Machine Intelligence Vol. 21, pp. 537-543, 1999.

[4] O. Bustos, S. Ojeda and R. Vallejos, “Spatial ARMA models and its applications to image filtering”, Brazilian Journal of Probability and Statistics, Vol. 23 (2), pp. 141-165, 2009.

[5] O. Bustos, S. Ojeda, M. Ruiz, R. Vallejos and A. Frery, “Asymptotic Behavior of RA-estimates in Autoregressive 2D Gaussian Processes”, Jounal of Statistical Planning and Inference, Vol. 139(10), pp. 3649-3664, 2009.

[6] B. Choi, “On the asymptotic distribution of mean, autocovariance, autocorrelation, crosscovariance and impulse response estimators of a stationary multidimensional random field”, Communications in Statistics- Theory and Methods, Vol. 29(8), pp. 1703-1724, 2000.

[7] B. R. Cullis and A. C. Glesson, “Spatial analysis of field experimentsan extension to two dimensions”, Biometrics, Vol. 47(4), pp. 1449-1460, 1991.

[8] C. Gaetan, and X. Guyon, “Spatial Statistics and Modelling”, Springer, New York, 2010.

[9] M. G. Genton and H. L. Koul, “Minimum distance inference in unilateral autoregressive laticce processes” Statistica Sinica, Vol. 18, pp. 617-631, 2008.

[10] M. R. Grondona, J. Crossa, P. N. Fox and W. H. Pfeiffer, “Analysis of variety yield trials using two-dimensional separable ARIMA processes”, Biometrics, Vol. 52(2), pp. 763-770, 1996.

[11] J. Guo and L. Billard, “Some inference results for causal autoregressive processes on a plane”, Journal of Time Series Analysis, Vol. 19(6), pp. 681 691, 1998.

[12] Image database, Signal and Image Processing Institute, University of Southern California, http://sipi.usc.edu/database/

[13] A. K. Jain, “Fundamentals of Digital Image Processing”, Prentice Hall.

[14] R. Kashyap and K. Eom, “Robust images techniques with an image restoration application”, IEEE Trans. Acoust. Speech Signal Process, Vol. 36(8), pp. 1313-1325, 1988.

[15] S. M. Ojeda, R. Vallejos and O. Bustos, “A New Image Segmentation Algorithm with Applications to Image Inpainting”, Computational Statistics & Data Analysis, Vol. 54(9), pp. 2082-2093, 2010.

[16] S. M. Ojeda, R. Vallejos and W. P. Lamberti, “Measure of Similarity Between Images Based on the Codispersion Coefficient”, Journal of Electronic Imaging, Vol. 21, 2012.

[17] R. Vallejos and G. Garcia-Donato, “Bayesian analysis of contaminated quarter plane moving average models”, Journal of Statistical Computation and Simulation, Vol. 76 (2), pp. 131-147, 2006.

[18] Ronny Vallejos and Silvia Ojeda, Chapter in book: “Segmentation of Images and Time Series Based on Spatial ARMA Processes”, Advances in Image Segmentation, October 24, 2012, ISBN 980-953-307-581-0.

[19] Z. Wang and A. Bovik, “A universal image quality index”, IEEE Signal Processing Letters, Vol. 9(3), pp. 81-84, 2002.

[20] Z. Wang and A. Bovik, “Modern Image Quality Assessment”, Morgan & Claypool Publishers, United States of America, 2006.